Supporting Information

Improved Desalination Performance of Flow- and Fixed-Capacitive Deionization using Redox-Active Quinone

Nguyen Anh Thu Tran[a], Ngo Minh Phuoc[a], Hana Yoon[b], Euiyeon Jung[c], Young-Woo Lee[a], Beom-Goo Kang[d], Hong Suk Kang[e,], Chung-Yul Yoo[f,]*, and Younghyun Cho[a,]**

[a]Department of Energy Systems Engineering, Soonchunhyang University, Asan 31538, Korea

[b]Korea Institute of Energy Research, 152 Gajeong-ro, Yuseong-gu, Daejeon 34129, Korea

[c]Department of Materials Science and Engineering, University of Pennsylvania, 3231 Walnut Street, Philadelphia, PA 19104, USA

[d]Department of Chemical Engineering, Soongsil University, Seoul 06978, Korea

[e]Interface Materials and Chemical Engineering Research Center Korea Research Institute of Chemical Technology, Daejon 34114, Korea.

[f]Department of Chemistry, Mokpo National University, Muan-gun, Jeollanam-do 58554, Korea

21 Pages, 15 Figures, and 4 Tables are included.

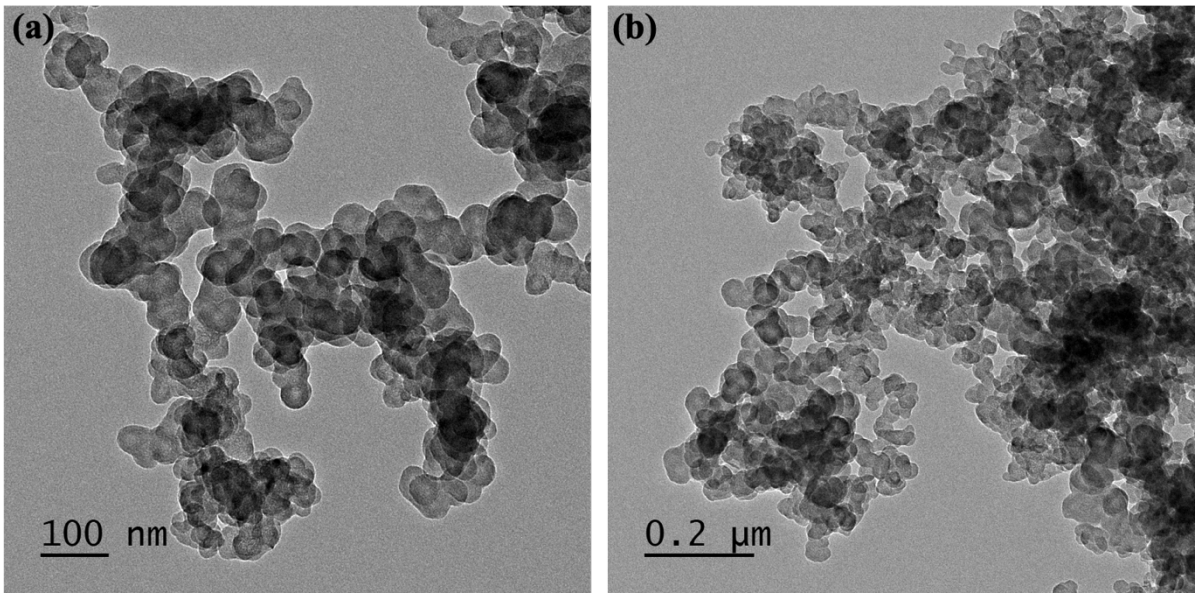

Figure S1. High- and low magnification TEM images of carbon black nanoparticles used in the present study.

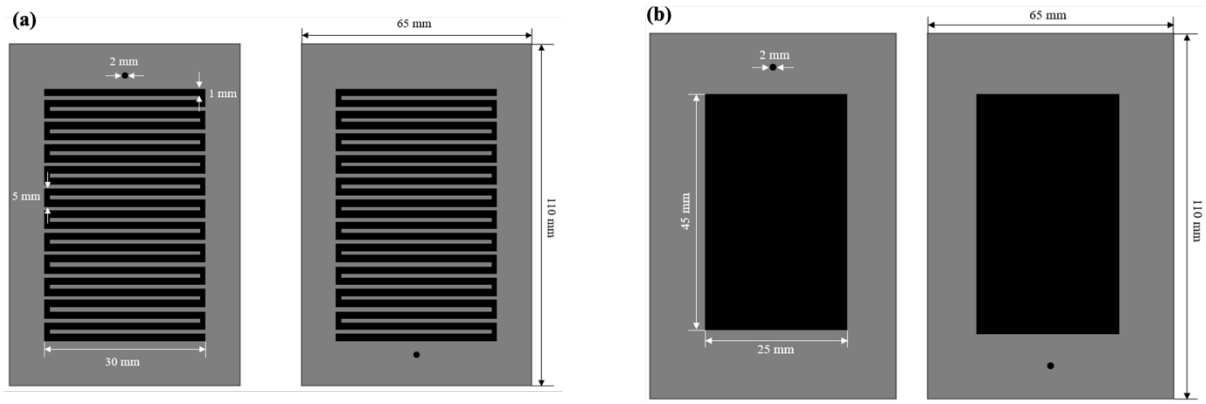

Figure S2. Schematics of graphite current collectors of (a) FCDI cell and (b) CDI cell used in the present study.

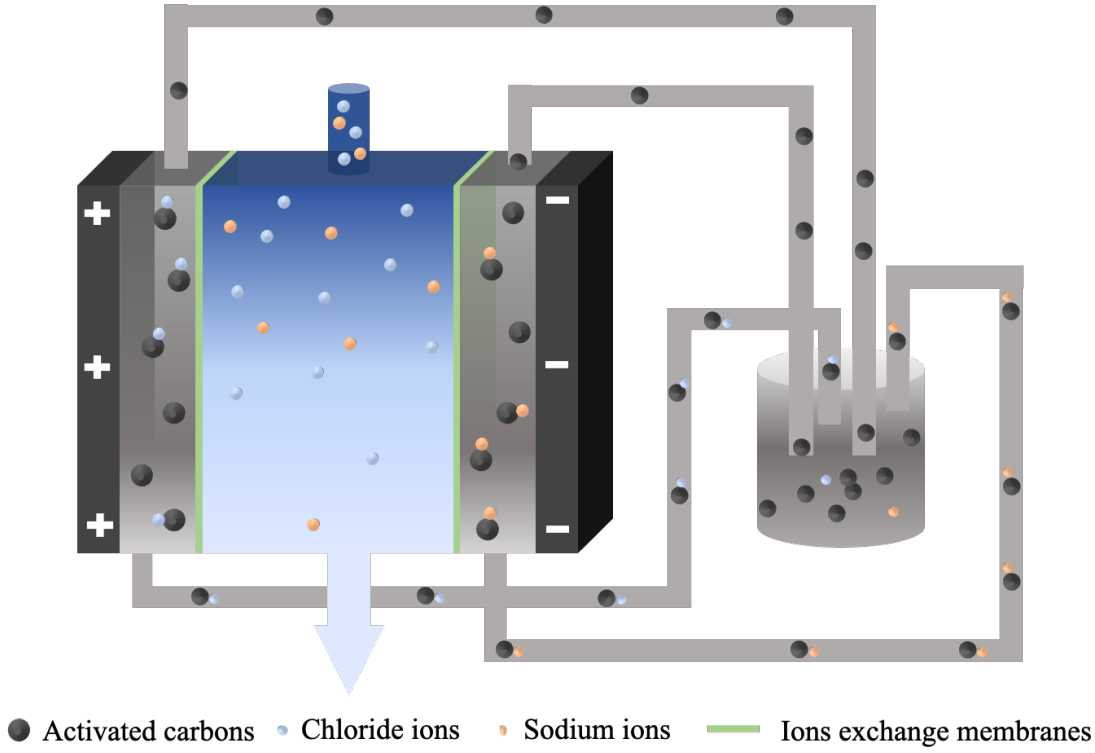

Figure S3. Schematic of FCDI cell configuration used in the present study (Short-circuited closed cycle mode).

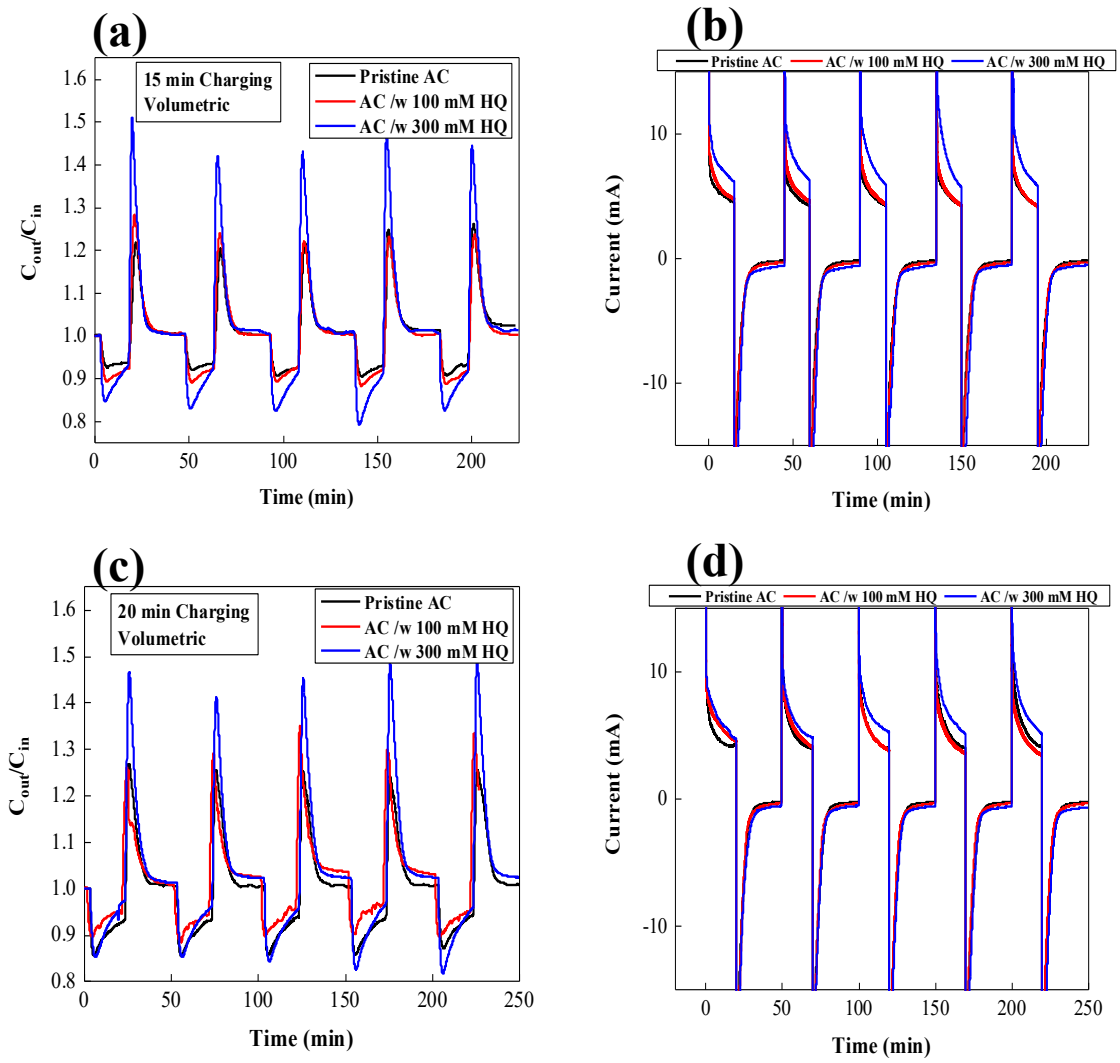

Figure S4. Changes in the salt concentrations of the effluent stream during CDI operation (volumetric comparison) at different charging times of (a) 15 min and (c) 20 min. Corresponding measured currents at different charging time of (b) 15 min and (d) 20 min.

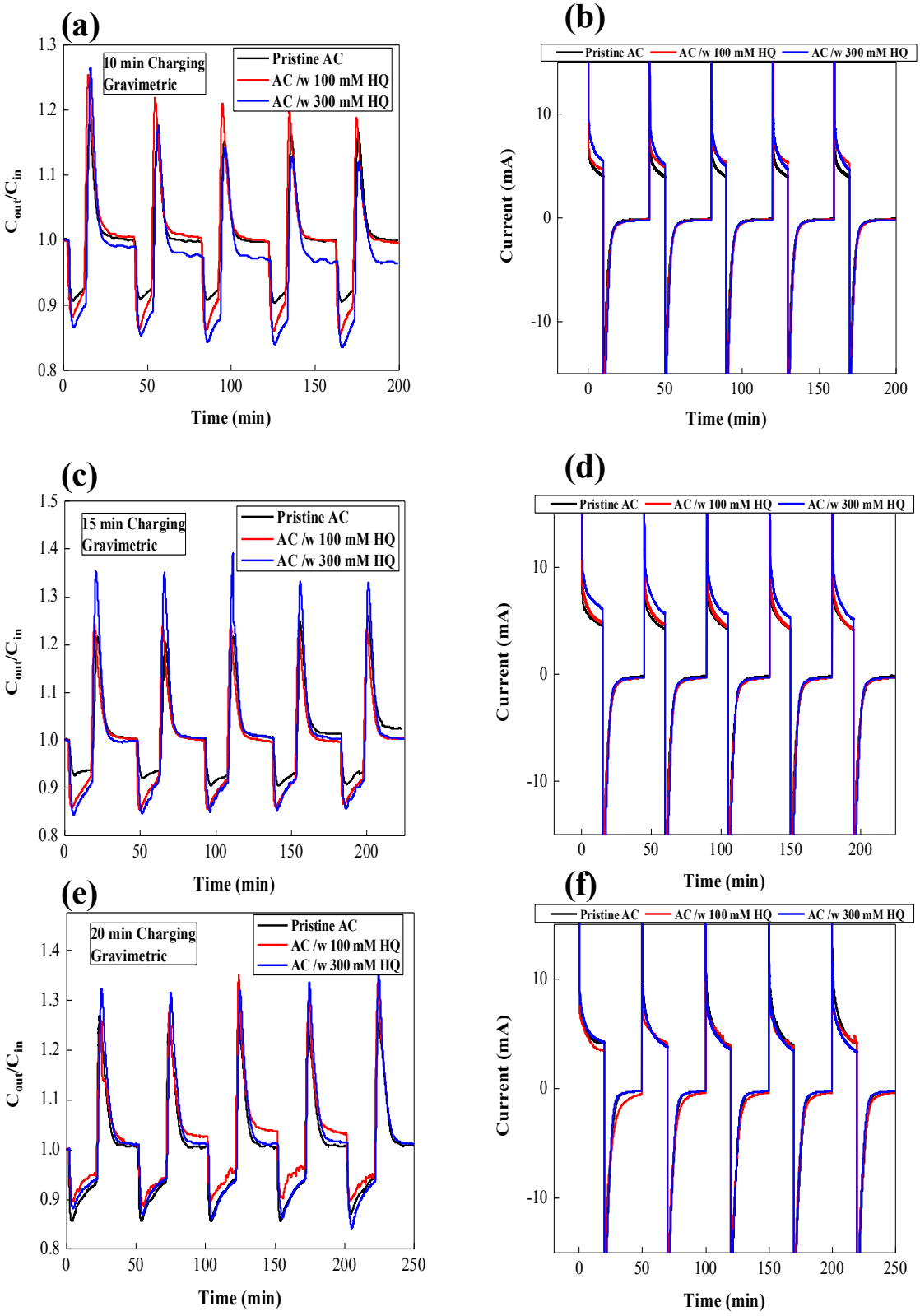
(a)
10 min Charging
Gravimetric
Pristine AC
AC /w 100 mM HQ
AC /w 300 mM HQ
C_{out}/C_{in}
Time (min)
(b)
Pristine AC
AC /w 100 mM HQ
AC /w 300 mM HQ
Current (mA)
Time (min)
(c)
15 min Charging
Gravimetric
Pristine AC
AC /w 100 mM HQ
AC /w 300 mM HQ
C_{out}/C_{in}
Time (min)
(d)
Pristine AC
AC /w 100 mM HQ
AC /w 300 mM HQ
Current (mA)
Time (min)
(e)
20 min Charging
Gravimetric
Pristine AC
AC /w 100 mM HQ
AC /w 300 mM HQ
C_{out}/C_{in}
Time (min)
(f)
Pristine AC
AC /w 100 mM HQ
AC /w 300 mM HQ
Current (mA)
Time (min)

Figure S5. Changes in the salt concentrations of the effluent stream during CDI operation (gravimetric comparison) at different charging times of (a) 10 min, (c) 15 min, and (e) 20 min, Corresponding measured currents at different charging time of (b) 15 min, (d) 15 min, and (f) 20 min.

Table S1. SAC and ASAR at the various experimental conditions for CDI desalination.

Charging Time (min)	**Parameters**	**Pristine AC**	**AC /w 100 mM HQ**		**AC /w 300 mM HQ**	
			Gravimetric	Volumetric	Gravimetric	Volumetric
10	SAC (mg/g)	4.35	4.41	4.92	6.14	7.37
15		5.22	5.97	5.97	7.21	7.99
20		6.81	7.64	7.95	8.20	8.33
10	ASAR (mg/g min)	0.44	0.47	0.49	0.62	0.74
15		0.35	0.40	0.40	0.48	0.53
20		0.34	0.38	0.39	0.41	0.42

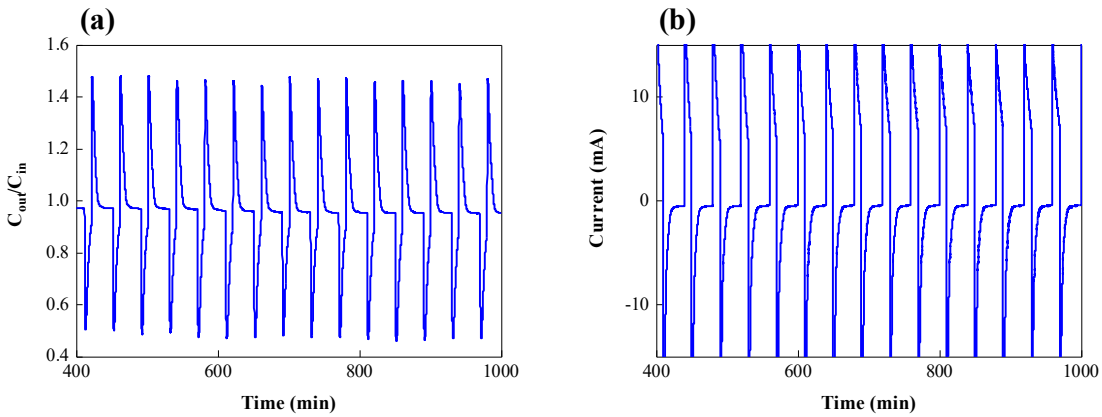

Figure S6. Variation in (a) the salt concentration of effluent stream and (b) measured current during CDI desalination using AC w/ 300 mM HQ for 15 cycles.

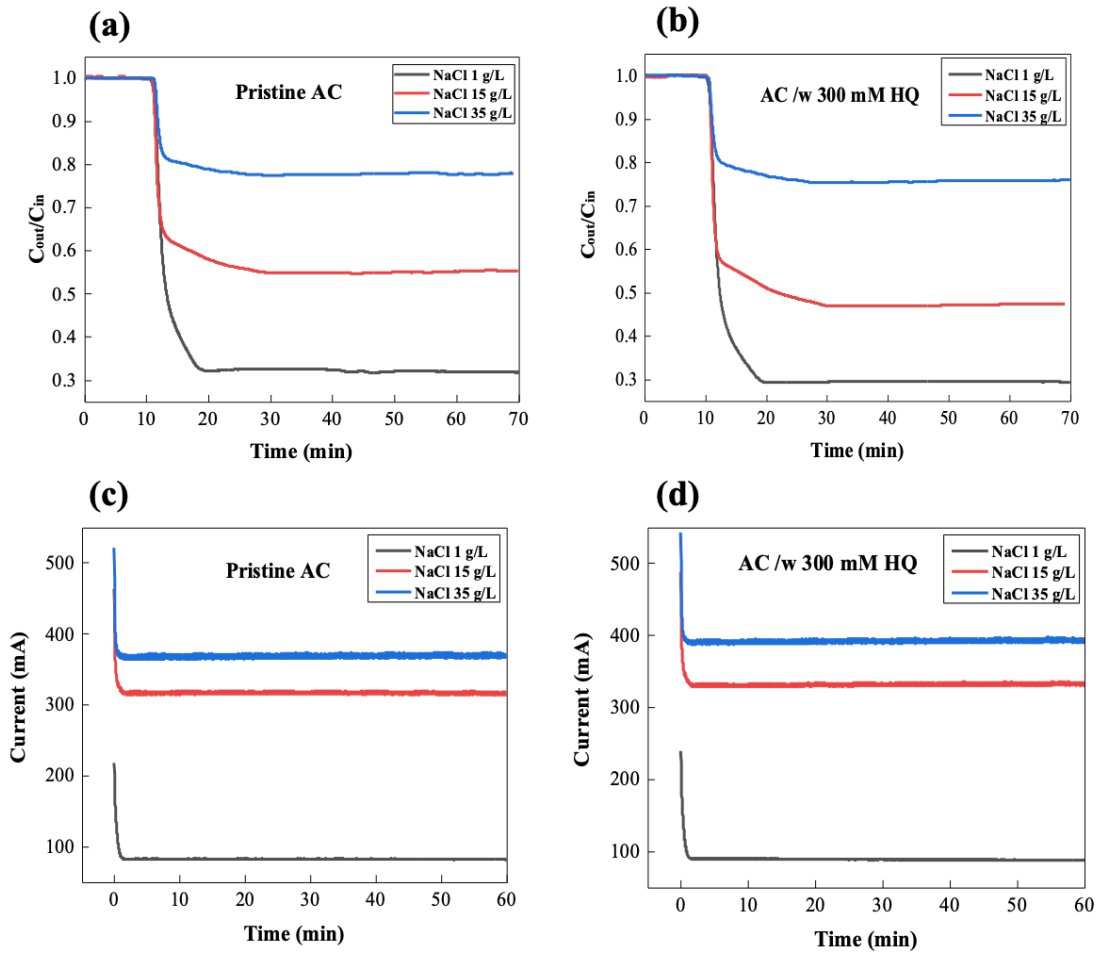

Figure S7. Changes in the salt concentration of the effluent stream during FCDI operation using (a) pristine AC and (b) AC /w 300 mM HQ as a function of feed concentration. Corresponding measured current during FCDI operation using (c) pristine AC and (d) AC /w 300 mM HQ.

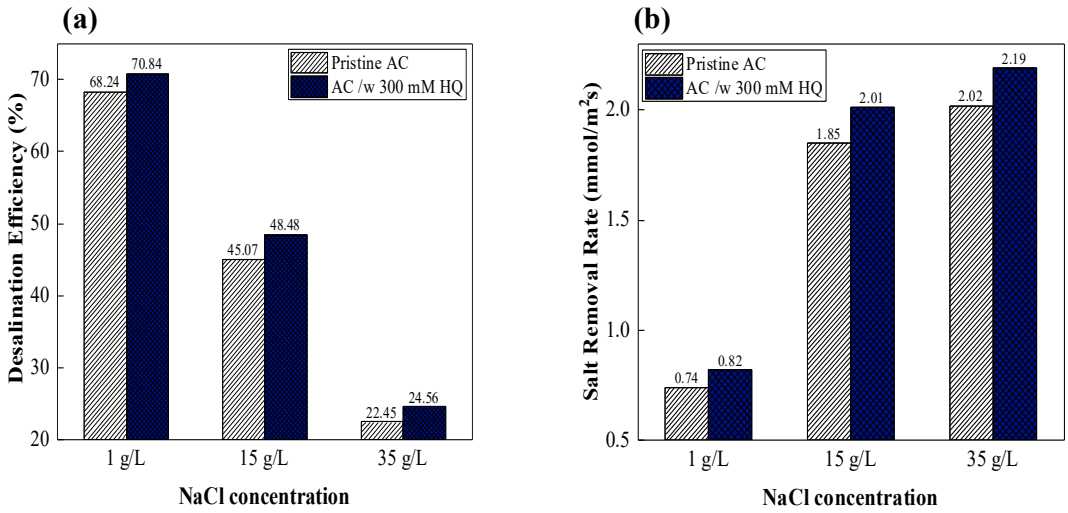

Figure S8. Change in (a) desalination efficiency and (b) salt-removal rate as a function of feed concentration.

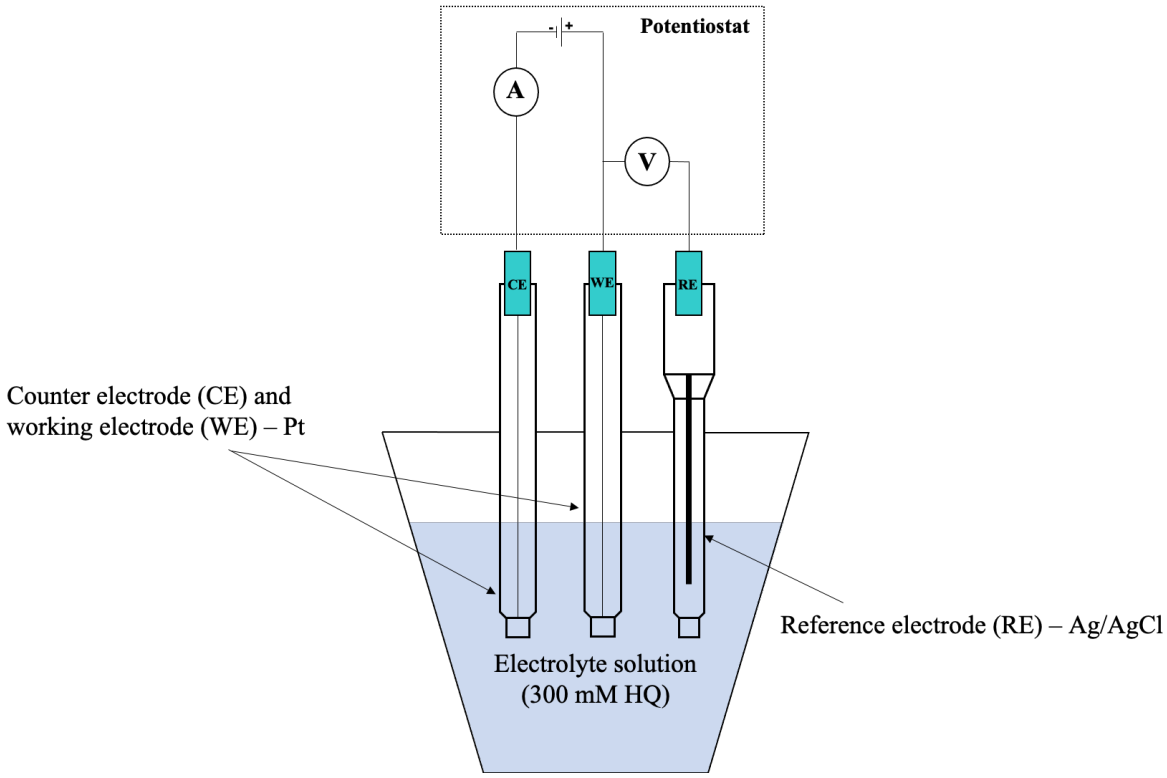

Figure S9. Schematic of CV measurement setup in three-electrode beaker cell using the 300 mM HQ without AC in a static mode.

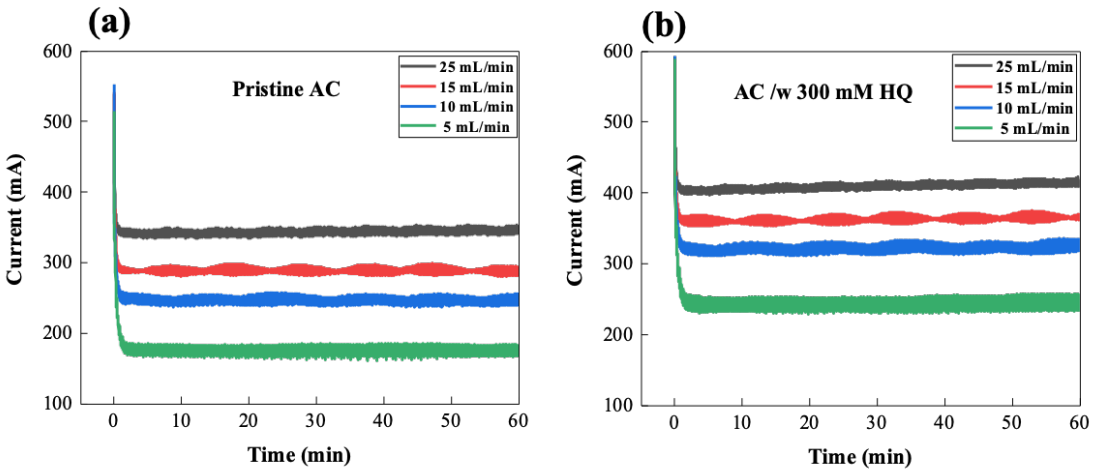

Figure S10. Changes in the measured current during FCDI operation using (c) pristine AC and (d) AC /w 300 mM HQ.

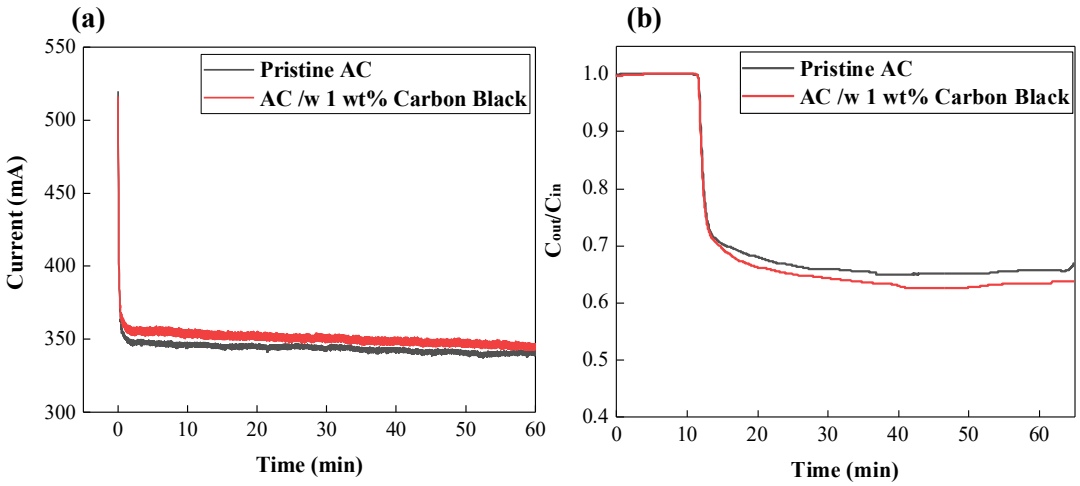

(c)

Type of electrode	Pristine AC	AC /w 1 wt% Carbon Black
Desalination efficiency (%)	35.2	37.4
Average salt removal rate (mmol/m²s)	2.92	3.15

Figure S11. Variation in (a) current and (b) the salt concentration of effluent stream during FCDI desalination using pristine AC and AC /w 1 wt% carbon black nanoparticles.

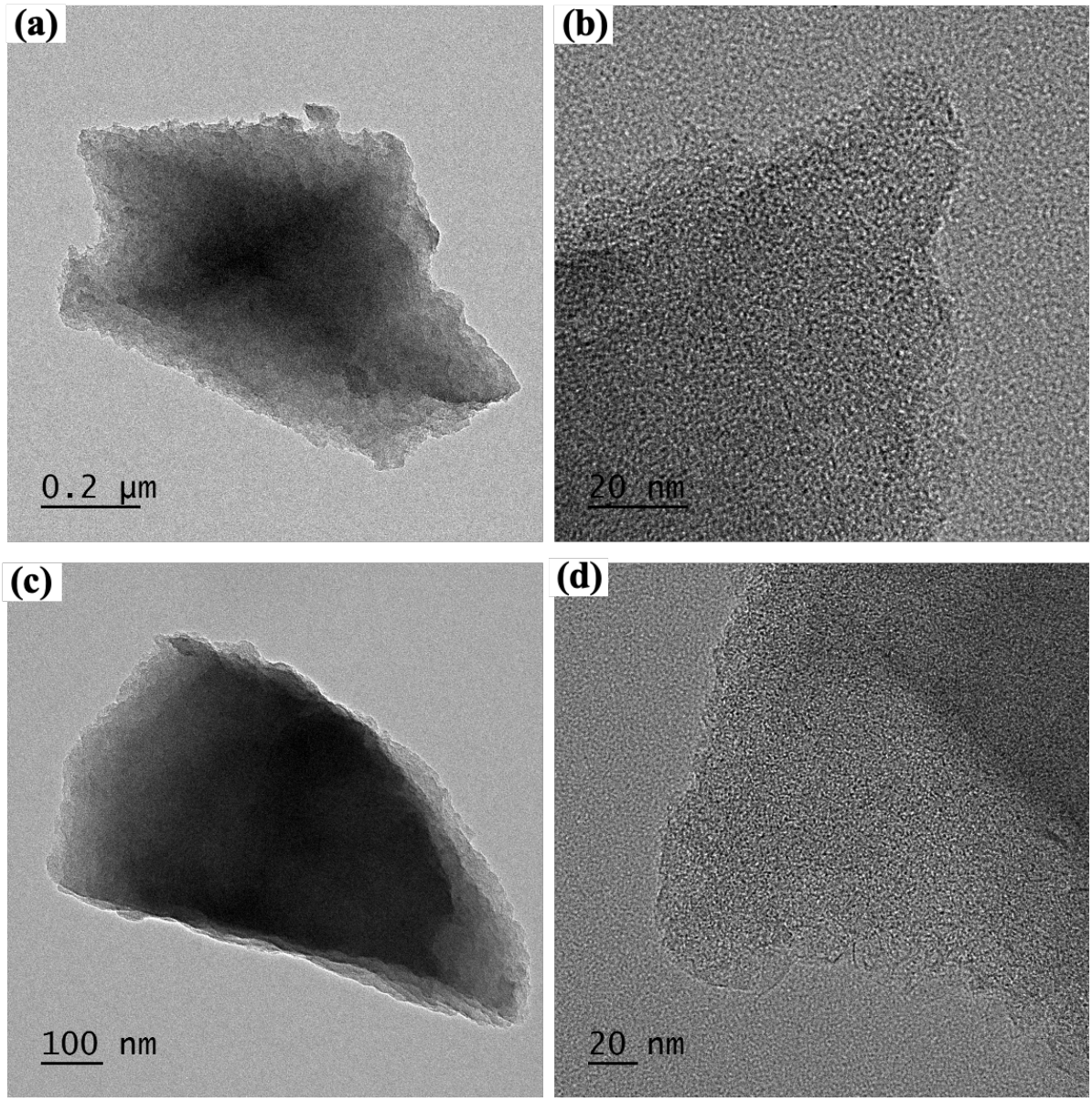

Figure S12. TEM images of (a) and (b) pristine AC and (c) and (d) AC /w HQ 300 mM HQ. (a) and (c) are the low- and (b) and (d) are the high-magnification images.

Table S2. Capacitance and specific capacitance calculated from Figure 5c.

Flow electrode	Pristine AC	AC /w 50 mM HQ	AC /w 300 mM HQ	HQ 300 mM w/o AC
Capacitance (F)	8.03	9.59	10.83	0.75
Specific Capacitance (F/g)	5.06	5.91	6.02	1.79

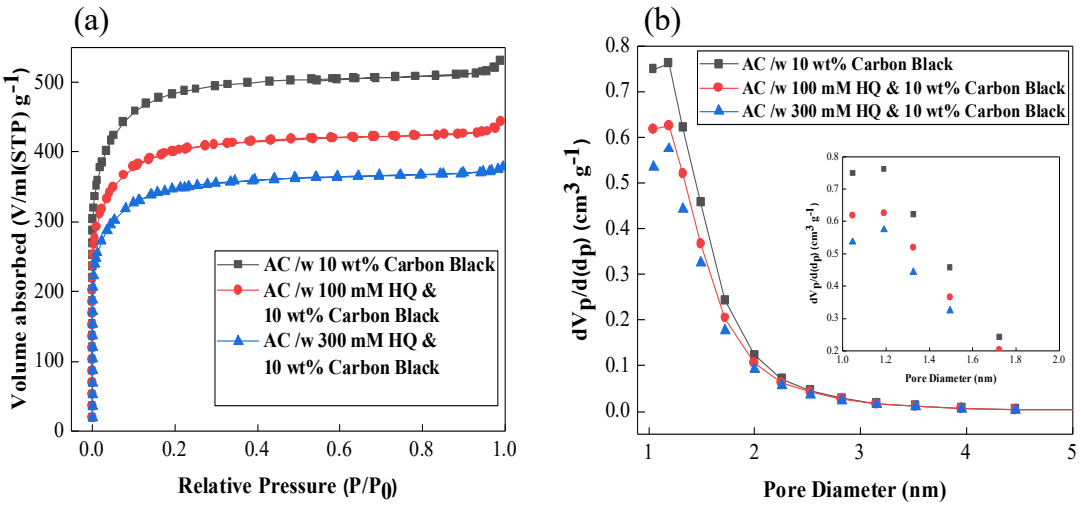

(c)

	SSA (m^2/g)	Pore Volume (cm^3/g)
AC /w 10 wt% Carbon Black	1827	0.82
AC /w 100 mM HQ & 10 wt% Carbon Black	1511	0.68
AC /w 300 mM HQ & 10 wt% Carbon Black	1229	0.58

Figure S13. (a) Nitrogen adsorption-desorption isotherms, (b) the pore-size distribution, and (c) specific surface area and pore volume of AC, AC /w 100, and 300 mM HQ & 10 wt% carbon black nanoparticles.

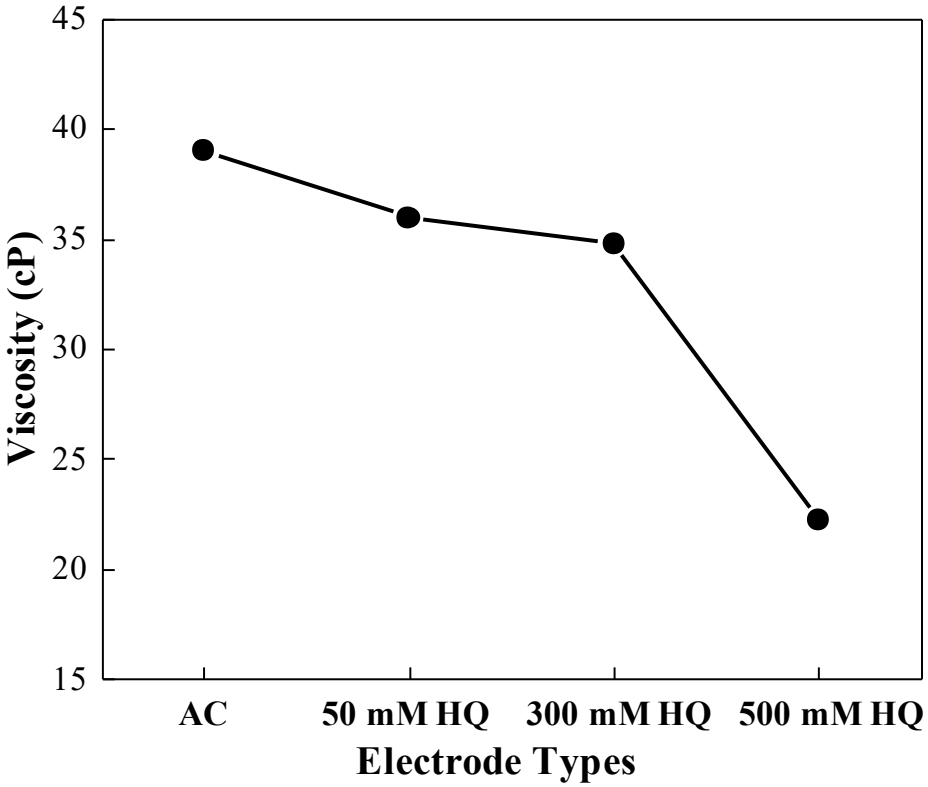

Figure S14. Change in viscosity as a function of HQ concentration.

Table S3. EIS fitting parameters for AC, 100 mM HQ, and 300 mM HQ for CDI operation.

	AC	**100 mM HQ**	**300 mM HQ**
R1 (Ω)	**10.77 (±0.01)**	**14.37 (±0.01)**	**12.04 (±0.01)**
R2 (Ω)	**2.88 (±0.01)**	**3.70 (±0.02)**	**2.57 (±0.04)**
CPE1 ($\Omega^{-1}\cdot s^{-n}$)	**1.72×10^{-2} ($\pm 2.63 \times 10^{-4}$)**	**1.40×10^{-2} ($\pm 2.30 \times 10^{-4}$)**	**1.13×10^{-2} ($\pm 5.30 \times 10^{-4}$)**
n1	**0.72 (±0.01)**	**0.75 (±0.01)**	**0.87 (±0.01)**
C (F)	**5.47×10^{-3}**	**5.17×10^{-3}**	**6.71×10^{-3}**
WO-R (Ω)	**5.14 (±0.07)**	**38.74 (±0.43)**	**74.63 (±1.51)**
WO-T (s)	**13.48 (±0.39)**	**25.59 (±0.65)**	**28.29 (±1.23)**
WO-P	**0.5**	**0.5**	**0.5**

Table S4. EIS fitting parameters as a function of HQ concentration for FCDI operation.

	AC	50 mM HQ	300 mM HQ	500 mM HQ
R1 (Ω)	**1.939 ($\pm 2.39 \times 10^{-3}$)**	**1.904 ($\pm 1.74 \times 10^{-3}$)**	**1.885 ($\pm 1.92 \times 10^{-3}$)**	**1.847 ($\pm 1.91 \times 10^{-3}$)**
R2 (Ω)	**1.096 ($\pm 1.01 \times 10^{-1}$)**	**0.908 ($\pm 4.99 \times 10^{-2}$)**	**0.912 ($\pm 6.61 \times 10^{-2}$)**	**1.036 ($\pm 9.09 \times 10^{-2}$)**
CPE1 ($\Omega^{-1} \cdot s^{-n}$)	**3.74×10^{-1} ($\pm 1.30 \times 10^{-2}$)**	**3.68×10^{-1} ($\pm 1.13 \times 10^{-2}$)**	**4.31×10^{-1} ($\pm 1.53 \times 10^{-2}$)**	**4.64×10^{-1} ($\pm 1.58 \times 10^{-2}$)**
n1	**0.441 (±0.009)**	**0.460 (±0.007)**	**0.446 (±0.008)**	**0.442 (±0.008)**
R3 (Ω)	**2.160 ($\pm 1.38 \times 10^{-1}$)**	**1.733 ($\pm 7.16 \times 10^{-2}$)**	**1.775 ($\pm 8.63 \times 10^{-2}$)**	**1.849 ($\pm 1.07 \times 10^{-1}$)**
CPE2 ($\Omega^{-1} \cdot s^{-n}$)	**1.783 ($\pm 1.92 \times 10^{-1}$)**	**2.217 ($\pm 1.55 \times 10^{-1}$)**	**2.140 ($\pm 1.75 \times 10^{-1}$)**	**2.008 ($\pm 1.91 \times 10^{-1}$)**
n2	**0.629 (±0.020)**	**0.653 (±0.015)**	**0.662 (±0.015)**	**0.680 (±0.016)**

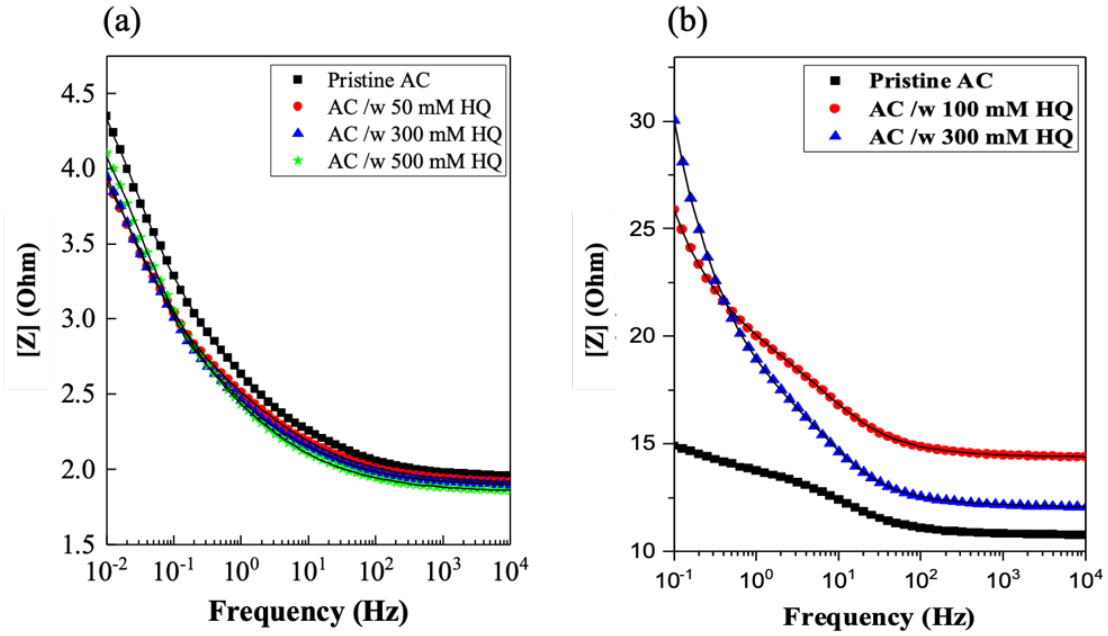

Figure S15. Bode plots of (a) FCDI and (b) CDI operation mode as a function of frequency.

In the case of FCDI, the impedance magnitude (|Z|) at 10^4 Hz gradually decreases to 1.96, 1.92, 1.90, and 1.86 Ω for higher HQ concentrations (for 0, 50, 300, and 500 mM HQ), respectively. The impedance magnitude at high frequency region mainly originates from the ion mobility in electrolyte phase rather than the ion penetration into the deeper intrapore of AC. Therefore, lower impedance at high frequency region in the presence of HQ indicates that HQ-BQ redox transformation efficiently acts as an electron mediator in flow electrode slurry. The impedance magnitude values at 10^{-2} Hz are 4.35, 3.91, 3.94, and 4.10 Ω for 0, 50, 300, and 500 mM HQ respectively. The impedance magnitude difference between 10^{-2} Hz and 10^4 Hz are 2.39, 1.99, 2.04, and 2.24 Ω for 0, 50, 300, and 500 mM HQ respectively. The impedance magnitude difference mainly originates from the electron transfer and ion adsorption and can be significantly affected by the HQ-BQ redox reaction and the coverage of AC with non-conductive HQ molecules, which is in good agreement with the variation in specific surface

area of AC (Figure 6). In the case of CDI, the impedance magnitude values are 10.78, 14.39, and 12.08 Ω at 10^4 Hz and 14.91, 25.86, and 29.98 Ω at 10^{-1} Hz for 0, 100, and 300 mM HQ respectively. From the variation of impedance magnitude at high frequency region, the presence of 100 mM HQ deteriorates the proton and electronic conductivity of AC, whereas the presence of 300 mM HQ enhances the proton and electronic conductivity of AC since the hydrogen bonding significantly occurs between HQ clusters allowing proton and electron transfer reaction between HQ clusters.[1] The impedance magnitude difference between 10^{-1} Hz and 10^4 Hz are 4.13, 11.47, and 17.90 Ω for 0, 100, and 300 mM HQ respectively. The impedance magnitude difference is comprised of both interfacial ion adsorption on AC and ion diffusion from the bulk electrolyte to electrolyte-AC interface. The interfacial ion adsorption resistance (R2 in Table S3) values are in the range of 2.57-3.70 Ω. Therefore, the increase of impedance magnitude difference with increasing HQ concentration is mainly due to the decrease of ion diffusion from the bulk electrolyte to the electrode–electrolyte interface into AC pore since the aggregated HQ clusters at the AC surface decreases the pore volume of AC (Figure 6). The ion diffusion coefficient is inversely proportional to the Warburg resistance (WO-R) and the square of time constant (WO-T) from the equivalent circuit fitting.[2] The increase of both Warburg resistance and time constant (Table S3) with increasing HQ concentration is in good agreement with the increase of impedance magnitude difference due to the decrease of ion diffusion into AC pore.

(1) Manojkumar, T. K.; Kim, D.; Kim, K. S.; Theoretical studies on hydroquinone-benzene clusters. *J. Chem. Phys.* **2005,** *122* (1).

(2) Yoon, H.; Kim, H. J.; Yoo, J. J.; Yoo, C. Y.; Park, J. H.; Lee, Y. A.; Cho, W. K.; Han, Y. K.; Kim, D. H.; Pseudocapacitive slurry electrodes using redox-active quinone for high-performance flow capacitors: an atomic-level understanding of pore texture and capacitance enhancement. *J. Mater. Chem. A* **2015,** *3* (46), 23323-23332.